

ARTICLE OPEN



Causes of 2022 Pakistan flooding and its linkage with China and Europe heatwaves

Chi-Cherng Hong¹, An-Yi Huang¹, Huang-Hsiung Hsu²✉, Wan-Ling Tseng^{1,3}, Mong-Ming Lu⁴ and Chih-Chun Chang¹

In boreal summer of 2022, Pakistan experienced extremely high rainfall, resulting in severe flooding and displacing over 30 million people. At the same time, heatwaves persisted over central China and Europe. The coexistence of these extreme events suggests a possible linkage. Our analysis indicated that the record rainfall was mainly induced by compounding factors. These included (1) La Niña-induced strong anomalous easterlies over the northern Indian subcontinent, (2) intense southerlies from the Arabian Sea with an upward trend in recent decades, (3) an interaction between extratropical and tropical systems, specifically the northerly flow downstream of the Europe blocking and the southerly monsoon flow from the Arabian Sea. Wave activity flux and regression analyses unveiled a distinct stationary Rossby wave-like pattern connecting the flooding in Pakistan and heatwaves in Europe and China. This pattern, an emerging teleconnection pattern in recent decade, exhibited substantial differences from the reported teleconnection patterns. We also noted the positive feedback of the excessive Pakistan rainfall could further enhance the large-scale background flow and the heavy rainfall itself. The 2022 Pakistan flood event was an intensified manifestation of the 2010 Pakistan flood event, which was also caused by compounding factors, but occurred in a more pronounced upward trend in the both tropics and extratropics.

npj Climate and Atmospheric Science (2023)6:163; <https://doi.org/10.1038/s41612-023-00492-2>

INTRODUCTION

In 2022, Pakistan experienced a sequence of unusually intense monsoon rainfall surges that struck from early July to late August. The extreme rainfall caused widespread landslides along the Indus River basin, resulting in flooding across one-third of the country. The flooding left over 30 million people homeless and resulted in 1000 deaths, as well as over USD 30 billion in damage and economic losses, according to the World Bank. The accumulated rainfall was approximately four standard deviations above the climatological mean value and was twice the amount of rainfall observed in the 2010 flooding event, which caused significant socioeconomic losses and nearly 3000 deaths. Concurrently, extreme heatwaves persisted over central China and Europe, severely affecting agriculture and power supply. The concurrence of these extreme events suggests a possible linkage¹.

The year 2022 witnessed a triple-dip La Niña that began in 2020. Previous studies have indicated that a La Niña summer tends to exhibit a strong western North Pacific Subtropical High (WNPSH) and Indian monsoon flow^{2–6}. The influence of La Niña-induced changes in large-scale circulation has been identified as a crucial factor in causing the 2010 extreme flooding event^{7,8} and likely had a similar impact in 2022. Although the Niño4 index reached an unusually low level during the boreal summer of 2022 (the second lowest since 1979, following 1999), the regression analysis of 850-hPa moisture flux on Niño4 and Niño3.4 (of moderate magnitude) individually did not exhibit substantial differences over the northern Indian subcontinent and Pakistan (not shown). This suggests that La Niña alone, including Niño4 SST, cannot fully explain the anomalous rainfall in Pakistan. For example, the total rainfall in 2022, despite having a moderate La Niña (Niño3.4), was nearly double that of the strong La Niña year in 2010. In addition,

extreme rainfall events did not occur in other La Niña summers, such as 1998 and 1999.

The extreme events of 2010 and 2022 exhibited notable similarities, in addition to occurring during La Niña conditions. The 2010 flooding in Pakistan, which ranked among the top three in terms of accumulated rainfall since 1979, was attributed to a tropical–extratropical interaction. This interaction involved a northerly flow associated with a blocking high and heatwave over Europe, coupled with an intensified summer monsoon flow in the western Indian Ocean (IO)^{7,9,10}. Similarly, in 2022, a strong blocking high and heatwave over Europe (45°–60°E) coincided with an intense summer monsoon in the Arabian Sea, observed from mid-June to late August. In both instances, the heatwave in Europe and the flooding in Pakistan were connected through an extratropical Rossby wave-like perturbation over the Eurasian continent. It is plausible that a comparable tropical–extratropical interaction contributed to the 2022 flooding in Pakistan. Furthermore, there is evidence of enhanced atmospheric perturbations and increasing sea surface temperatures (SST) in recent decades, which may have intensified extreme rainfall and heatwaves^{11–14}. SST in the IO has been rising since 1980^{15,16}, and higher SST levels contribute to increased moisture availability and strengthened moisture transport, potentially amplifying rainfall over mountainous regions in Pakistan. Understanding whether this trend played a role in the heavier rainfall observed in 2022 is therefore essential.

Extreme events have been reported to occur when different influencing factors synchronized^{12,17,18}. In this study, we explore the physical processes that led to the record rainfall in Pakistan in 2022 (Fig. 1a). Our focus is especially on the above-mentioned compounding effect on the extreme rainfall in 2022. Additionally, we address the linkage of the record rainfall with the Europe and

¹Department of Earth and Life Science, University of Taipei, Taipei, Taiwan. ²Anthropogenic Climate Change Center, Research Center for Environmental Changes, Academia Sinica, Taipei, Taiwan. ³International Degree Program in Climate Change and Sustainable Development, National Taiwan University, Taipei, Taiwan. ⁴Department of Atmospheric Sciences, National Taiwan University, Taipei, Taiwan. ✉email: hhsu@gate.sinica.edu.tw

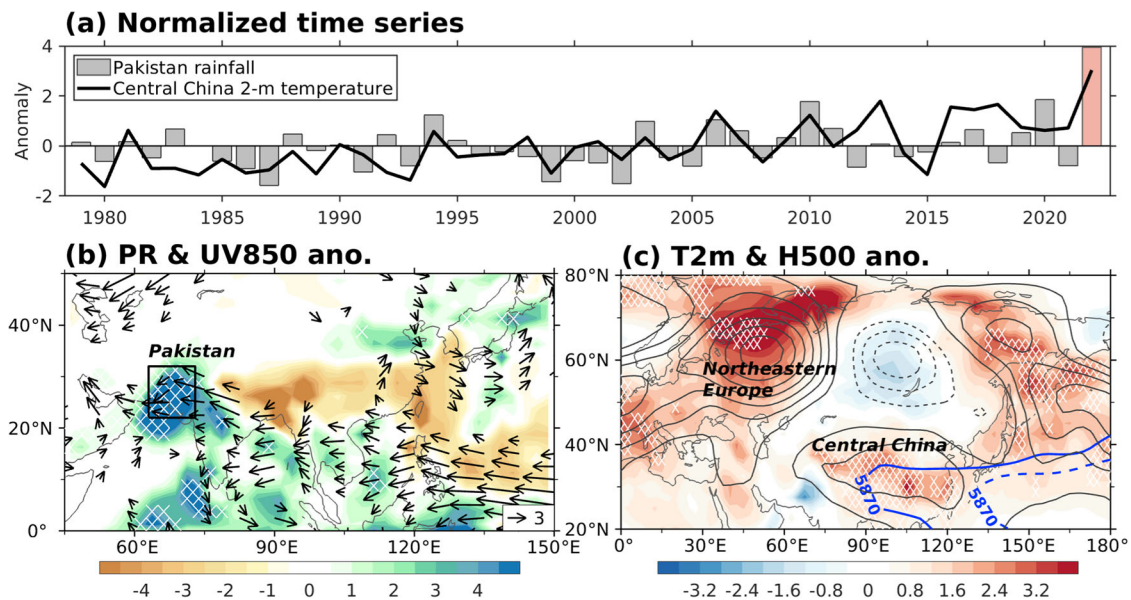


Fig. 1 Large-scale conditions during the 2022 Pakistan extreme rainfall events. **a** Normalized time series of July–August averaged Pakistan (PKT; 22°–32°N, 63°–73°E) rainfall index (one standard deviation equals 1.31 mm day⁻¹) and Central China 2-m temperature (T2m; 25°–35°N, 90°–120°E) index (one standard deviation equals 0.58 °C). The correlation coefficient between PKT rainfall and Central China T2m indices is 0.44 ($P < 0.01$) during 1979–2021. **b** July–August averaged anomalous precipitation (PR, shading; unit: mm day⁻¹) and 850-hPa horizontal winds (UV850, vectors; unit: m s⁻¹; minimum vector: 1). Black box indicates the region for Pakistan rainfall index. **c** Same as in (b), except the shading and black contour lines represent the near-surface temperature (T2m; unit: °C) and 500-hPa geopotential height (H500; unit: m; interval: 15) anomalies, respectively. Blue solid and dashed contour lines (5870-m isoline) are the 2022 and climatological mean of 500-hPa geopotential height, respectively, representing the location of WNPSH. Shadings with white crosses in both (b, c) indicate that the signals (precipitation and 2-m temperature) of each grid exceeded the 99th percentile during 1979–2022.

China heatwaves. Our hypothesis posits that the flooding was caused by compounding factors: the unusually strong anomalous easterlies induced by La Niña over the northern Indian subcontinent, an enhanced southerly flow from the Arabian Sea characterized by an upward trend in recent decades, and the tropical–extratropical interaction between monsoon and northerly surges. Even more intriguingly, we identify a Rossby wave-like teleconnection pattern over the Eurasian continent, which has been in action since 2010, that connected the Pakistan’s record rainfall to the China and Europe heatwaves.

RESULTS

Features of the record rainfall in Pakistan

Figure 1a depicts the time series of July–August averaged rainfall in Pakistan and China’s 2-meter temperature (T2m) from 1979 to 2022. In addition, Fig. 1 presents the anomalous rainfall, T2m, 850-hPa wind, and 500-hPa geopotential height (H500) over the Eurasian continent in 2022. In 2022, both Pakistan and northwestern India experienced rainfall that exceeded the 99th percentile value based on the 1979–2022 data. Central China and northeastern Europe, downstream and upstream of Pakistan, respectively, witnessed below-normal rainfall and above-normal T2m values that exceeded the 99th percentile (Fig. 1b, c). The extreme rainfall in Pakistan was accompanied by an intensified southwesterly flow from the Arabian Sea and an easterly anomaly associated with the strong Western North Pacific Subtropical High (WNPSH) extending from the western North Pacific (WNP) to the northern Indian subcontinent. The convergence of the anomalous southwesterly and easterly winds near Pakistan provided a favorable large-scale condition for convection. At the same time, anomalous anticyclonic circulations and extreme warmth resided over Europe and China.

The daily time series of the Pakistan (PKT) rainfall index (Fig. 2a) reveals three unusually strong monsoon rainfall surges during

July–August 2022. During these surges, strong southerly flows originating in the Arabian Sea reached Pakistan and converged with the anomalous southward-penetrating northerly flow from the extratropics (Fig. 2b). The first surge occurred in early to mid-July, followed by the second surge in late July, and the third, the strongest event, persisted from early to late August. Notably, both the first and third surges were accompanied by the northward propagation of convection from the Arabian Sea and the southward penetration of northerly from the extratropics toward Pakistan (Fig. 2c), a phenomenon also observed during the other two extreme events in 2010 and 2020 (Supplementary Fig. 1c, g). The three monsoon rainfall surges accounted for ~32%, 16%, and 49%, respectively, of the accumulated rainfall from July to August, collectively contributing to more than 90% of the total rainfall during that period. Consequently, a record accumulated rainfall of 450-mm was observed from July 1st to August 31st, which was approximately four times higher than the climatological average and twice as much as the previous record set in 2010. Understanding the first and third surges was particularly important because of their significant contribution to total rainfall and also the common influences by both southerly and northerly surges. Although a short-lived tropical storm occurred in the Arabian Sea on 12–13 August, it did not make landfall and thus did not significantly contribute to the observed excessive rainfall. The excessive rainfall in August was primarily attributed to the third monsoon surge¹⁹.

A mid-to upper-level blocking high was observed over northeastern Europe (Fig. 1c), similar to 2010⁷. The blocking high was particularly pronounced in August (Fig. 2d) and accompanied by enhanced trough (downstream of the blocking) and northerly winds extending southward from extratropical Eurasia to South Asia (Fig. 2b). The anomalous northerly flow transported cold-dry air southward, creating a convection-favorable environment (i.e., an unstable atmosphere) near Pakistan when it met the tropical warm-moist southerly flow from the Arabian Sea⁷. This tropical–extratropical interaction was also observed in 2010 and

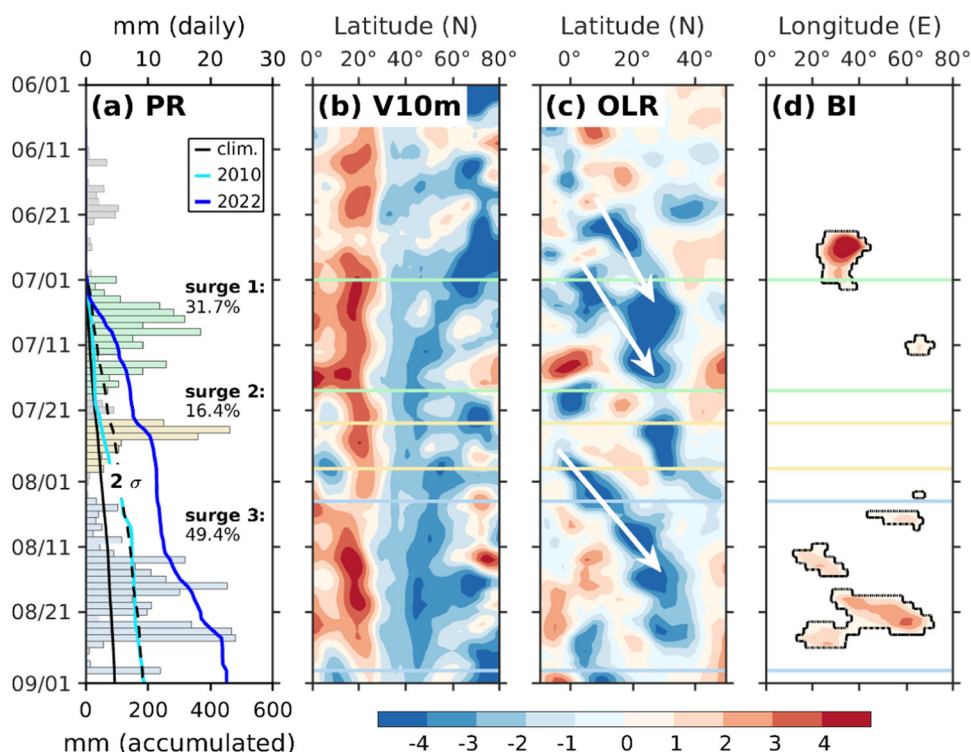


Fig. 2 Time evolution of 2022 Pakistan extreme rainfall and associated large-scale conditions (from June 1st to September 1st). **a** Bars and lines represent daily and accumulated PKT rainfall (PR; unit: mm day^{-1}), respectively. The colored bars indicate three extreme rainfall periods (surge 1 in green: 7/1–7/18, surge 2 in yellow: 7/23–7/30, and surge 3 in blue: 8/4–8/30). The numbers near colored bars are the percentage of the accumulated rainfall in each period against total period (7/1–8/31). **b** Hovmöller (time-latitude) diagram of 3-day averaged 10-m meridional wind (V10m, shading; unit: m s^{-1}) averaged over 60° – 75° E. **c** Same as (b), but for anomalous outgoing longwave radiation (OLR, shading; unit: 10^1 W m^{-2}). White arrows indicate the northward propagation of convection. **d** Hovmöller (time-longitude) diagram of blocking index with shading representing the 500-hPa geopotential height gradient south of middle-high latitude (blocking index, BI; unit: m/degree latitude ; only values larger than 0 are plotted) averaged over five grid points (details are documented in the methods section). Black contour lines (0 isoline) mark the regions of blocking.

likely played a significant role in inducing the extreme rainfall. These characteristics were most evident during the first and third monsoon surge, coinciding with the arrival of the northerly wind anomaly at Pakistan from the deepened trough downstream of the extratropical positive height anomalies (Fig. 2b, d). Our analysis showed that the Rossby wave-like perturbations over Eurasia occurred during the first and third rainfall surge. Their appearances were consistent with the duration of the rainfall event. That is, the pattern was persistently present in August but was relatively transient in July, especially during 5–11 July when large rainfall occurred (Supplementary Fig. 2).

All-time top 3 and top 1 rainfall events in Pakistan occurred, respectively, in 2010 and 2022. Both were La Niña years with anomalously low-level easterly winds over South Asia, an enhanced WNPSH, and an extratropical wave-like perturbation over Eurasia. However, they also differed in certain characteristics as discussed below. First, in 2022, a negative Indian Ocean Dipole (IOD)-like SST anomaly (SSTA) occurred, with warmer sea surface temperatures in the eastern IO, whereas in 2010, a basin-wide warm SSTA was observed in the IO (Fig. 3a, b). Second, an unusually persistent upper-level anticyclone anomaly was present over central China in 2022 (Fig. 3a), while in 2010, positive anomalies appeared over central Eurasia and near Japan²⁰ (Fig. 3b).

The 2022 event exhibited several distinctive features: record-breaking rainfall, the presence of La Niña, a strong and westward-extended WNPSH, a strong southerly flow over the Arabian Sea, an easterly anomaly over the northern Indian subcontinent, an upper-level trough associated with upstream Europe blocking, and vigorous tropical–extratropical interaction. To assess the

rareness of these factors, we compared the circulation and sea surface temperature (SST) characteristics of the 2022 event with those of the 2010 and 2020 extreme events (exceeding 1.5 standard deviation of Pakistan rainfall) as well as the La Niña years in 1998 and 1999 (with 1 negative standard deviation of Niño3.4 but lower Pakistan rainfall) (Supplementary Fig. 3). The comparisons are summarized in Supplementary Table 1.

An enhanced WNPSH and associated lower-level easterly anomalies extending from the WNP to the northern Indian subcontinent were observed in 1998, 2010, 2020, and 2022, but not in 1999 (Supplementary Fig. 4). The La Niña-associated SSTA in the eastern equatorial Pacific contributed to the enhancement of the WNPSH^{21,22} in 1998, 1999, 2010, and 2022. In addition, the easterly anomaly associated with the WNPSH, extending from the WNP to the IO, indicates a weakened southwesterly monsoon flow, which could enhance moisture convergence and rainfall in Pakistan and northwestern India. Nevertheless, in the La Niña summers of 1998 and 1999, Pakistan received less rainfall than normal. In contrast, the summer rainfall in Pakistan in 2020, a non-La Niña summer, was comparable to that in 2010 (Supplementary Fig. 3).

Notably, while the July–August averaged Niño4 SST in 2022 was the second lowest (following 1999) since 1979, the regression of 850-hPa moisture fluxes on Niño4 and Niño3.4 show only minor differences over Pakistan and the northwestern Indian subcontinent (not shown). The correlation between the PKT index and Niño3.4 was even higher than that with Niño4, suggesting an unusually low Niño4 in 2022 was not an important factor as might be suspected. These findings suggest that the La Niña SSTA alone seemed insufficient to cause the extreme rainfall in Pakistan, even

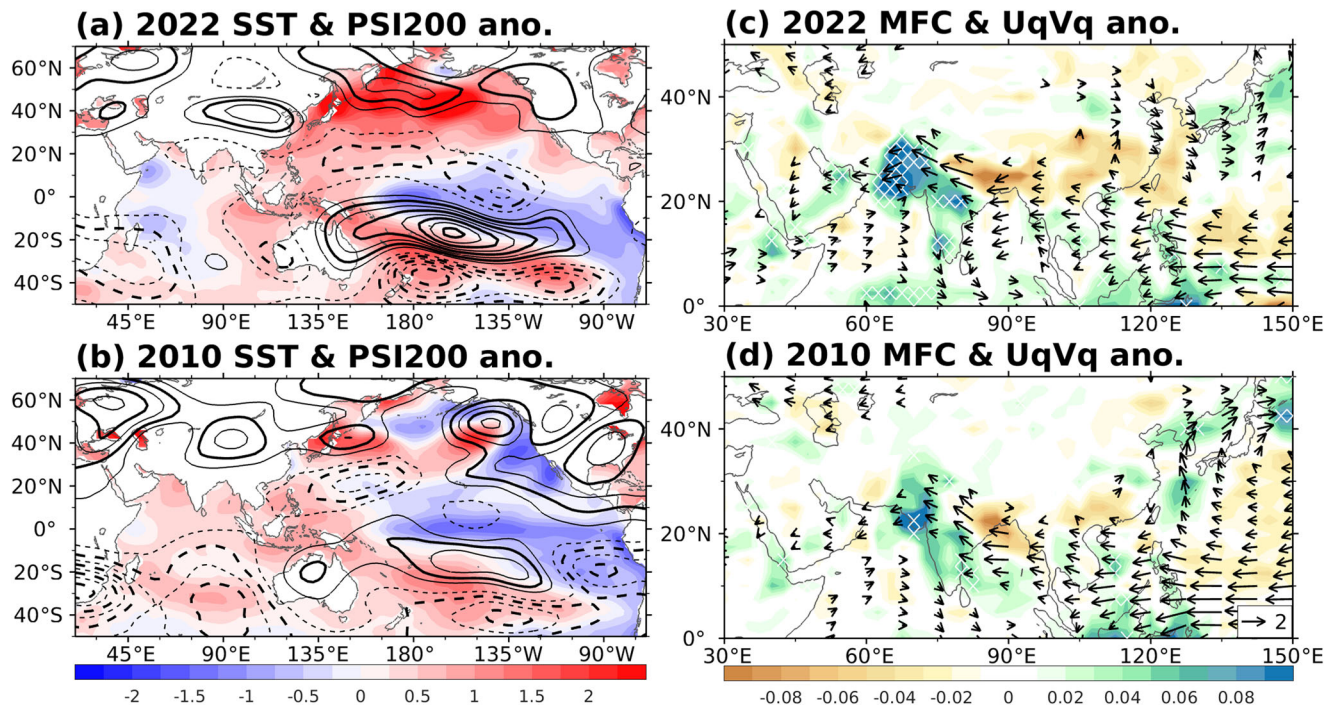


Fig. 3 Comparison of July–August averaged anomalous background conditions during two Pakistan extreme rainfall events in 2022 and 2010. **a** Sea surface temperature (SST, shading; unit: °C) and 200-hPa stream function (PSI200, contour; unit $10^6 \text{ m}^2 \text{ s}^{-1}$; interval: 3) in 2022. **b** Same as (a), but for 2010. **c** Vertically integrated (surface–300-hPa) moisture flux convergence (MFC, shading; unit: $\text{g m}^{-2} \text{ s}^{-1}$) and moisture flux (UqVq, vectors; unit: $10^5 \text{ g m}^{-1} \text{ s}^{-1}$; minimum vector: 0.4) in 2022. Note that the values of MFC had been multiplied by “-1” (i.e., positive and negative values represent convergence and divergence, respectively). **d** Same as (c), but for 2010. Shadings with white crosses in both (c, d) indicate the MFC exceeding the 99th percentile during 1979–2022.

though the summer Indian monsoon flow was suggested to be statistically stronger in La Niña years compared to neutral years^{23–25}. Similarly, the SSTa in the Indian Ocean, which exhibited distinct characteristics among the extreme rainfall summers of 2010, 2020, and 2022, did not seem to be an influential factor.

Furthermore, a clear tropical–extratropical interaction, similar to that observed in 2022, was identified in the extreme rainfall summer of 2010 (also a La Niña year), whereas it was absent in the two other La Niña years, 1998 and 1999 (not shown). This observation highlights the significant role of Europe-blocking-related wave activity in enhancing the tropical–extratropical interaction that contributed to the occurrence of extreme rainfall. These findings indicate that the extreme rainfall events in Pakistan during the summers of 2010 and 2022 were the result of multiple factors, including the La Niña-related enhancement of the WNPSH and the interaction between the tropical monsoon flow and extratropical disturbances. However, the reasons behind the higher rainfall in 2022 compared to 2010 remain unclear and are discussed in the following section.

Influencing factors

Climate extremes are often induced by compounding factors^{18,26}, and the summer of 2022 happened to be a summer in which the following factors coexisted.

Previous studies have revealed that the negative SSTa in the equatorial eastern Pacific during a La Niña summer²⁴ can induce an anticyclonic anomaly (i.e., a typical Gill-type response) in the WNP. This anticyclonic anomaly substantially weakens the southwesterly flow in South and East Asia^{25,27}. Consequently, the southwesterly flow becomes predominantly confined over the Arabian Sea, leading to enhanced moisture convergence and creating a more favorable environment for heavy rainfall in the northwestern Indian subcontinent. However, the above interpretation does not provide an explanation for why the total rainfall in

2022 was nearly double that of 2010, considering that the La Niña was slightly stronger in the boreal summer of 2010 than 2022.

One may suspect that the IO SSTa contributed to the stronger moist southwesterly flow over the Arabian Sea in 2022 compared to 2010 (Fig. 3c, d). As mentioned earlier, while both 2010 and 2022 were La Niña summers, they exhibited distinct characteristics in terms of IO SSTa (Fig. 3a, b). The question remains whether the negative IOD in 2022 resulted in a stronger southwesterly flow. Our calculation of the correlation coefficient (cc) between the 850-hPa meridional wind over the Arabian Sea (averaged over 10° – 20°N , 50° – 65°E) and the IOD index yielded a statistically insignificant 0.03 correlation ($P=0.83$, calculated based on Fisher’s Z-transformation). Therefore, the enhanced southwesterly in 2022 cannot be solely attributed to the negative IOD.

The tropical–extratropical interaction was another crucial factor in helping induce the record rainfall (Fig. 2). This interaction was particularly evident during the third surge, which persisted throughout almost the entire month of August. The third rainfall surge occurred when the northerly wind associated with the upstream blocking converged with the southerly flow over Pakistan (Fig. 2). This convergence resulted in strong convection in Pakistan.

In addition, our numerical experiment suggests that the convection-induced diabatic heating near Pakistan may accelerate the southerly flow from the Arabian Sea (Supplementary Fig. 5a), indicating a self-amplification between convection and circulation. A recent study reported that the atmospheric river from the Arabian Sea played a dominant role in the record rainfall over Pakistan in August¹⁹. Our study, in line with their findings, suggests the possibility that southward-penetrating extratropical disturbances helped trigger precipitation in Pakistan through tropical–extratropical interaction, which, in turn, could enhance the southerly flow (atmospheric river) from the Arabian Sea. This

positive feedback process could be a key feature in explaining the heavy rainfall observed in 2022.

The same mechanism can also be applied to the 2010 event, and therefore it cannot explicitly explain the heavier rainfall in 2022. However, we observed larger moisture flux over the northern Indian subcontinent and the Arabian Sea, as well as greater convergence near Pakistan during 2022 compared to 2010.

Considering the compatible La Niña (slightly weaker but more persistent in 2022) and the strength of the WNPSH in 2010 and 2022, another possibility for the heavier rainfall in 2022 is the long-term trends commonly observed in many regions and variables. While the summer rainfall in Pakistan does not exhibit a significant trend (Supplementary Fig. 6a), the moisture fluxes show a significant increasing trend in the Arabian Sea over 1979–2021 (Supplementary Fig. 6b). Calculations reveal a significant correlation between Pakistan rainfall and the southerly flow in the Arabian Sea ($cc = 0.32$, $P < 0.05$) during 1979–2021. When considering the contribution of the linear trend, the correlation coefficient increases to 0.41 ($P < 0.001$). Our analysis indicates that the increasing trend contributes approximately 21% of the total anomalous moisture flux convergence over Pakistan (Supplementary Fig. 7), potentially intensifying the rainfall. Particularly revealing features are the long-term trend of moisture flux over the Arabian Sea and from the Bay of Bengal to the northern Indian subcontinent, which led to the significant moisture flux convergence trend over Pakistan and northwestern India.

Furthermore, anticyclonic and warming trends have been observed over the western and eastern Eurasian continent. The anticyclonic trend in the eastern Eurasian continent is associated

with an easterly flux trend over the northern Indian subcontinent (Supplementary Fig. 6b, c). When removing the linear trend from the 2022 anomalies, we observe weaker anomalous highs over Europe and central China, as well as a weaker low-level easterly anomaly south of the Tibetan Plateau (Supplementary Fig. 6d–f). These findings suggest that the recent trends have contributed to both the observed Eurasian anomalies and the extreme rainfall in Pakistan.

The intensifying trend of the southerly moisture flux over the Arabian Sea is likely a result of the enhanced land–sea contrast and the warming Arabian Sea in recent decades (Supplementary Fig. 6b, c). The extratropical land has experienced faster warming compared to the ocean, particularly in central Asia, the Arabian Peninsula, and the Arabian Sea (Supplementary Fig. 6c). This increased land–sea contrast is speculated to lead to a stronger southerly flow over the Arabian Sea, allowing it to penetrate further into central Asia and the Arabian Peninsula. With the warmer SST in the Arabian Sea that would encourage more evaporation, the moisture flux trend could become even more significant. The intensified moisture transport from the Arabian Sea, combined with the lifting effect of the topography, could create strong upward motion near mountains (Supplementary Fig. 8), making a significant contribution to the rainfall in Pakistan.

Linkage between the flooding in Pakistan and heatwave in China and Europe

Another distinct feature of the 2022 Pakistan flooding is the linkage with the heatwaves in Europe and China (Fig. 4) through the Rossby wave-like perturbations over Eurasia. The linkage with

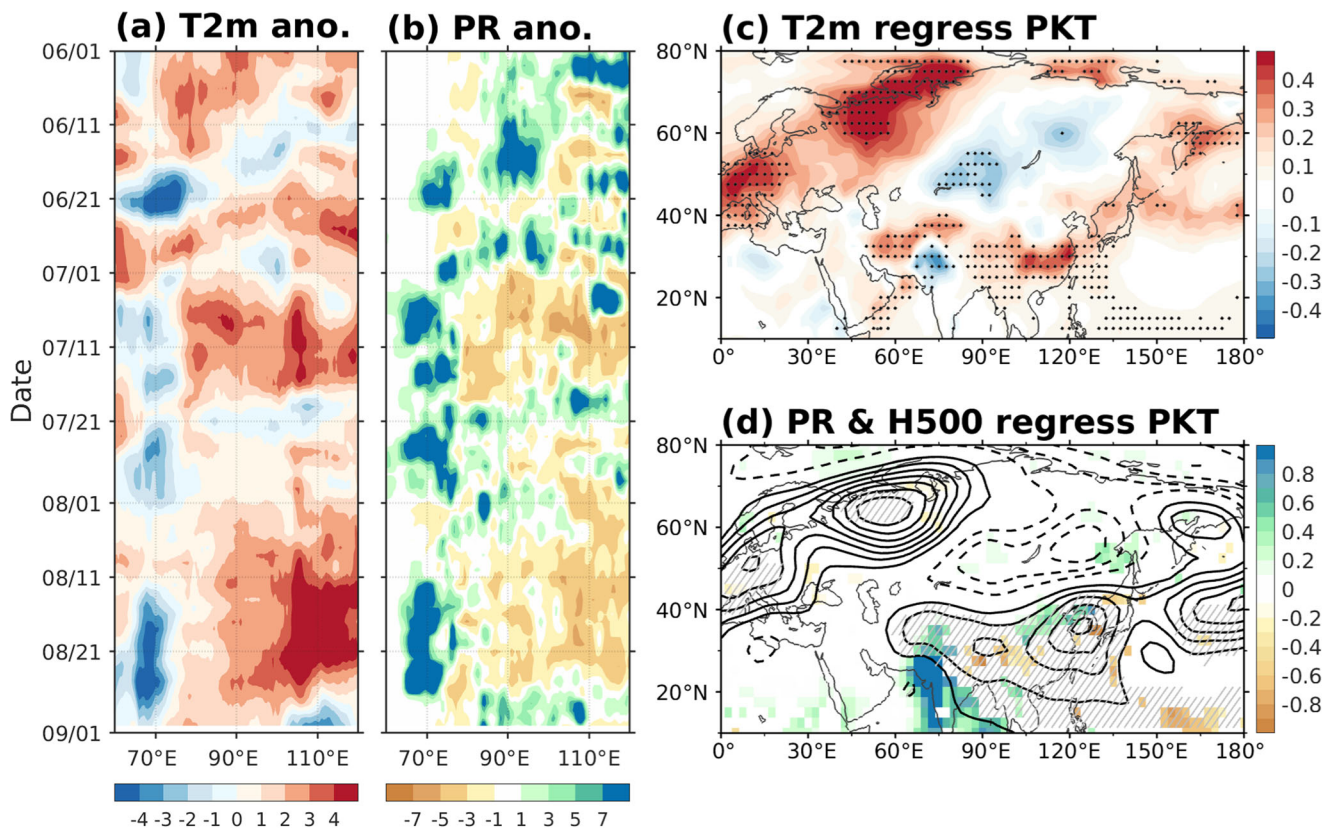


Fig. 4 Linkage between Pakistan rainfall and the heatwaves in China and Europe. **a** Hovmöller diagram of daily 2-m temperature (T2m, shading; unit: °C) anomaly (with 3-day moving mean) averaged over 25°–35°N during June–August 2022. **b** Same as (a), but for precipitation (PR, shading; unit: mm day⁻¹). **c** Regression coefficients of July–August averaged T2m (shading) on the normalized PKT index during 1979–2021. Black dots indicate the regression coefficients exceeding 90% confidence level based on Student's *t* test. **d** Same as (c), but for precipitation (shading) and 500-hPa geopotential height (contour; interval: 1.5). Shadings and slashed regions indicate the regression coefficients exceed 90% confidence level based on Student's *t* test.

the European heatwave was noted in the 2010 event⁷. The Pakistan rainfall was also connected with an East Asian heatwave in 2010²⁸. However, the heatwaves primarily occurred in north-eastern Asia (i.e., Korea and Japan), and the strength and coverage of heatwaves were much weaker and smaller, respectively, compared to 2022. In comparison, the linkage with the central China heatwave in 2022 was a more special characteristic. Figure 4a, b shows Hovmöller diagrams (averaged over 25°–35°N) of anomalous T2m and precipitation in 2022, respectively. The flooding in Pakistan (63°–73°E) was accompanied by a negative T2m anomaly (90°–120°E). In contrast, an opposite situation occurred in central China. The correlation coefficient between PKT rainfall and central China T2m (25°–35°N, 90°–120°E) indices is 0.44 ($P < 0.01$) during 1979–2021.

In the subsequent analysis, we regressed T2m, precipitation, and geopotential height in the Eurasian continent upon the July–August average rainfall index over Pakistan (Fig. 4c, d). A teleconnection pattern of the temperature and geopotential height, extending from Europe to East Asia, reveals that the Pakistan rainfall was significantly correlated with the T2m and geopotential height fluctuations in central China and northeastern Europe, where heatwaves occurred in 2022. Specifically, the PKT rainfall index was temporally correlated with averaged T2m and H500 over central China (25°–35°N, 90°–120°E; T2m: $cc = 0.44$, $P < 0.01$; H500: $cc = 0.57$, $P < 0.0001$) and northeastern Europe (60°–70°N, 40°–60°E; T2m: $cc = 0.33$, $P < 0.05$; H500: $cc = 0.28$, $P < 0.1$). Notably, the T2m in central China was highly correlated with the spatially-based heatwave index (see “Methods”; $cc = 0.79$, $P < 0.0001$), which also showed a significant correlation with the PKT rainfall ($cc = 0.39$, $P < 0.01$). In addition, the rainfall in Pakistan was significantly correlated with negative precipitation anomalies in central China and with positive anomalies in South Asia and northern China. The teleconnection pattern shows a close resemblance to observed anomalies in 2022, indicating that the connection between climate anomalies in Europe and Asia in 2022 did not occur coincidentally; instead, it has existed for more than four decades but emerged more strongly in 2022.

We further investigated whether the observed anomalies simply reflected a known teleconnection pattern. The first possibility is the Scandinavia (SCA) pattern^{29,30}, which has previously been reported to influence the heatwaves in northeast Asia³¹ (Supplementary Fig. 9a). However, the high-latitude anomalies (with positive anomaly centered ~50°E and negative anomaly centered ~100°E) in 2022 (Fig. 1c) exhibit an eastward shift compared with the SCA pattern (with positive anomaly centered ~20°E and negative anomaly centered ~80°E), and the SCA pattern shows no significant correlation with Pakistan rainfall ($cc = -0.08$, $P = 0.60$). Another candidate is the circumglobal teleconnection (CGT) pattern (Supplementary Fig. 9b), which occurred in the Northern Hemisphere during boreal summer³². While the CGT is also significantly correlated with Pakistan rainfall ($cc = 0.41$, $P < 0.01$), its spatial structure differs from that of the 2022 event and the long-term regression shown in Fig. 4d. For example, the wave-like pattern of the CGT upstream of Pakistan is shifted westward by about 50° longitude compared to the 2022 anomaly (Fig. 1c) and the regressed pattern (Fig. 4d). In addition, we noted some similarities between the regression pattern and the British–Okhotsk Corridor (BOC) pattern³³. However, there are distinct differences, such as the shorter wavelength (or spatial scale) and the northward shift of the negative anomaly toward Siberia in the BOC pattern compared to the PKT regression pattern. A series of calculation of 25-year sliding correlation, anomaly pattern correlation coefficient, and comparison of pattern characteristics with the BOC were conducted. Whereas the relevance between the two cannot be entirely ruled out, the comparison did not yield the conclusion that the PKT regression pattern was the reflection of the BOC. Our study reveals that the CGT, Scandinavia, and BOC pattern could not clearly explain the

PKT pattern. Whether it is an emerging pattern having increasing influences on Pakistan and China precipitation is noteworthy and warrants further investigation.

Analysis of wave activity flux³⁴ revealed an extratropical stationary Rossby wave-like perturbation in July and August. In July, the wave-like perturbation primarily propagated its energy eastward in high latitudes (Fig. 5a). By contrast, the perturbation in August originated from the Europe blocking, propagated south-eastward to central Asia and central China, and then turned northeastward toward the extratropical North Pacific (Fig. 5b). Positive stream function anomalies (i.e., blocking or ridges) were associated with heatwaves in Europe and China, while negative anomalies (i.e., deepened troughs) were associated with third monsoon surge, contributing approximately half of Pakistan rainfall. Whereas the wave-like pattern in July exhibited different characteristics, perturbations similar to that in August, and a regression pattern did exist in early July during the first rainfall surge (e.g., 5–11 July, Supplementary Fig. 2). The regression pattern prevailed persistent through August but appeared more transiently in July. As a result, the monthly mean in July exhibited different distributions. These findings indicate that the heatwaves and flooding in 2022 were linked by anomalous Rossby wave-like activity, in August and in certain period of July when heavy rainfall occurred in Pakistan.

A recent study has also reported the importance of Rossby wave-like teleconnection in linking Pakistan (western South Asia) and China (East Asia)¹. This study argued that the anomalous upper-level anticyclone associated with the China heatwave creates an easterly anomaly in its southern flank. This easterly flow, exceptionally strong and reversing the climatological westerly flow in the subtropical Tibetan Plateau, corresponds to anomalous ascending and descending motions in the eastern (Pakistan) and western (China) Tibetan Plateau, respectively. The observed ascending (descending) motion aligns with the anomalous rainfall (heatwave) in Pakistan (China). This interpretation however did not reveal causality. Our simulation partially supported this argument by demonstrating that the diabatic heating over Pakistan, likely in response to upstream wave activity from Europe, can induce an anticyclonic anomaly over central and southwest China, thereby sustaining the ridging activity and heatwave in China (Supplementary Fig. 5b). However, the model response exhibits a low-level westerly anomaly south of the Tibetan Plateau, consistent with the near-field baroclinic vertical structure response. This suggests a weakening effect on the observed low-level easterly flow, which is more likely associated with the typical equivalent barotropic vertical structure of extratropical perturbations.

Supplementary Fig. 5 also indicates that excessive precipitation in Pakistan can enhance the observed anticyclonic anomaly over China, Pakistan, and the Middle East, and also the southwesterly flow in the Arabian Sea. This result suggests that whereas the Pakistan heavy rainfall was induced by compounding effects of several influencing factors, its excessive heating could have positive feedback to further enhance the observed anomalies and heavy rainfall itself. The 2022 Pakistan flooding seemed to be a result of complicated and intertwined large-scale features and local heating that interacted rigorously. Further comprehensive investigations, employing carefully designed numerical experiments, are necessary to precisely identify the underlying physical processes.

DISCUSSION

In this study, we investigated the causes of the record rainfall in Pakistan during the boreal summer of 2022 and its linkage to the heatwaves in Europe and China. The record rainfall event was characterized by three distinct monsoon surges, which involved the northward propagation of deep convection from the Arabian

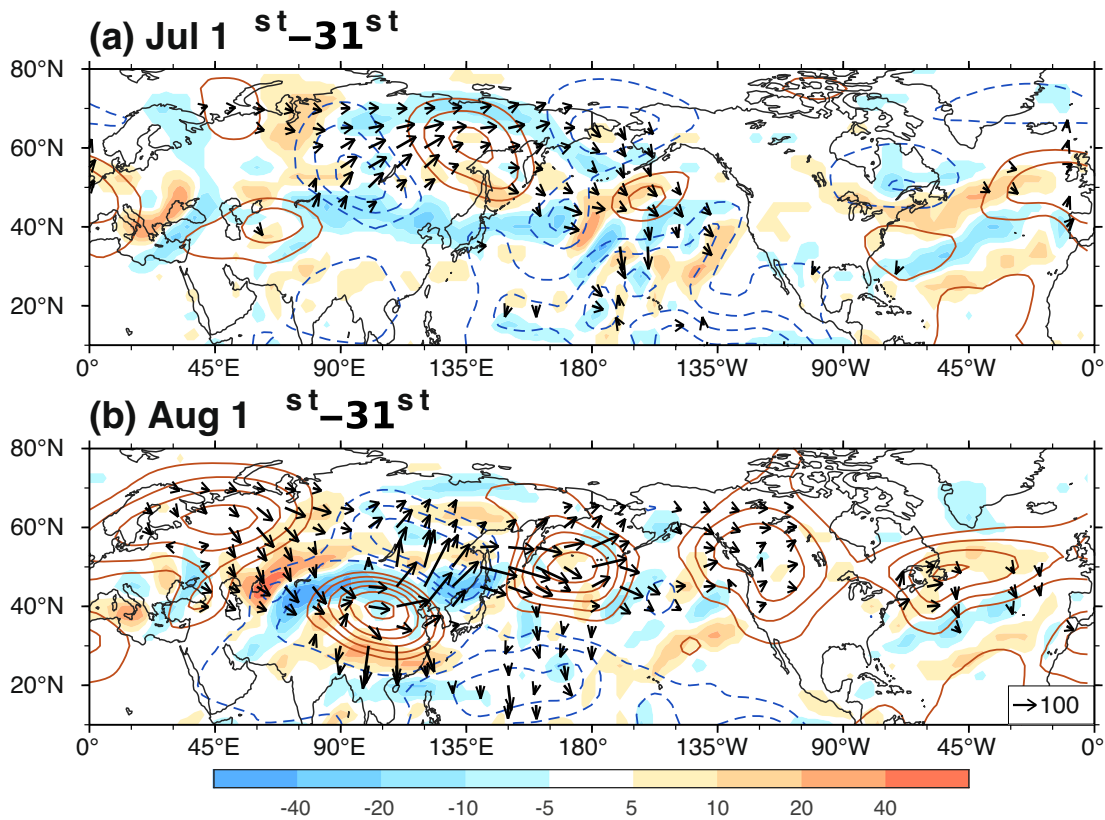


Fig. 5 Rossby wave source and wave activity flux. **a** July 1st to 31st averaged anomalous 200-hPa Rossby wave source (shading; unit: 10^{-11} s^{-2}), stream function (contour; unit: $10^6 \text{ m}^2 \text{ s}^{-1}$; interval: 3) and wave activity flux (vectors; unit: $\text{m}^2 \text{ s}^{-2}$; minimum vector: 25). **b** Same as (a), but for August 1st to 31st.

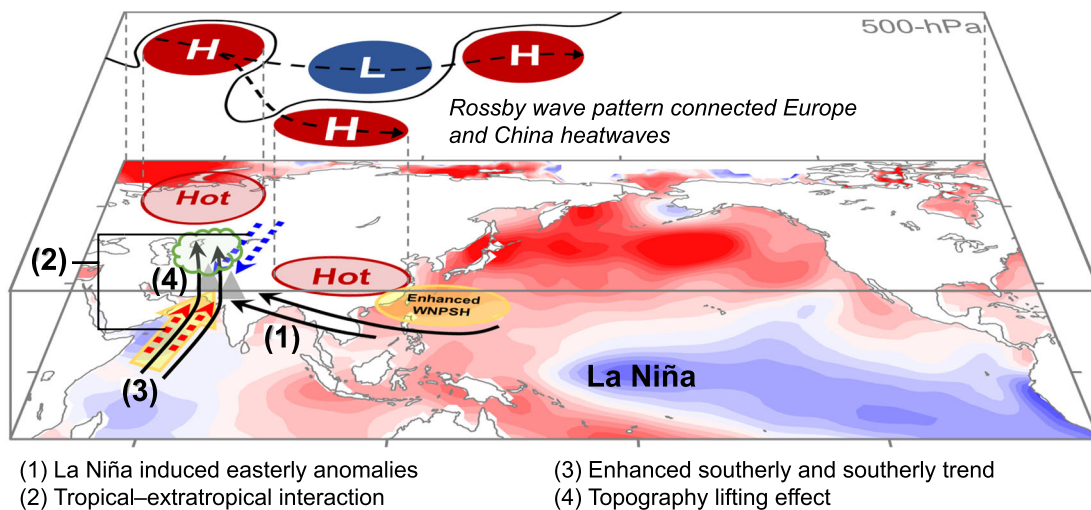


Fig. 6 Schematic diagram to present the main results of this study. (1) La Niña enhanced the WNP SH and the low-level easterly anomalies (black arrows). (2) Tropical-extratropical interaction: Europe blocking-associated cold-dry northerly wind (blue dotted arrows) converged with the warm-wet southerly flow (red dotted arrows) over Pakistan. The H-L-H indicates the high-level atmospheric teleconnection pattern linking Europe and China heatwaves and Pakistan flooding, which appeared persistently in August and more transiently in July when heavy rainfall occurred in Pakistan. (3) Enhanced southerly from the Arabian Sea, which was intensified by an upward trend in recent decades (yellow large arrow under red dotted arrows). (4) Topographic lifting effect (black arrows with upward curve) intensified upward motion over Pakistan. The gray-filled triangles represent mountains.

Sea. Our analysis revealed that multiple large-scale factors contributed to the occurrence of these extreme rainfall events, as schematically illustrated in Fig. 6. The compounding effects of influencing factors were similar to those identified for the 2010

Pakistan flooding. It could be viewed as an intensified manifestation of the 2010 Pakistan flooding event under a warming trend.

The unusually strong easterly anomaly induced by La Niña over the northern Indian subcontinent, along with an enhanced

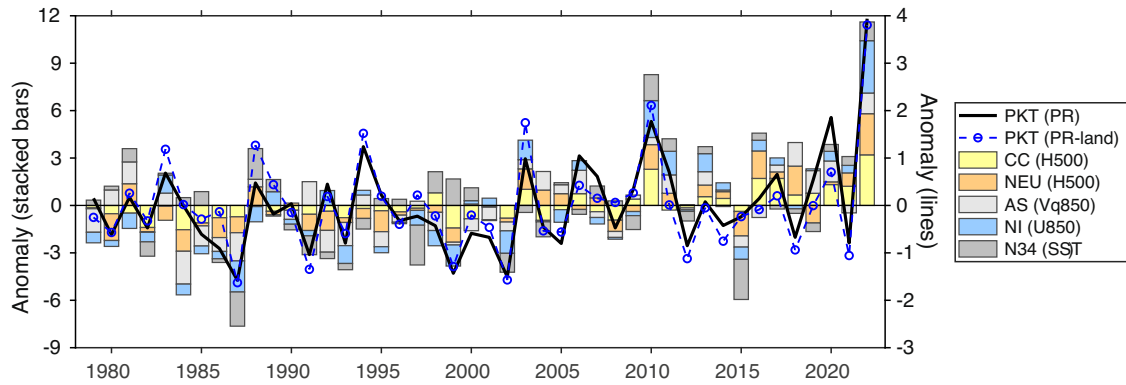


Fig. 7 Compounding effects of multiple influencing factors. The stacked bars (refer to left y axis) are normalized indices of 500-hPa geopotential height (H500) averaged over Central China (CC; 25°–35°N, 90°–120°E; yellow), H500 averaged over Northeastern Europe (NEU; 55°–70°N, 35°–60°E; orange), 850-hPa meridional moisture flux (Vq850) over Arabian Sea (AS; 5°–20°N, 55°–70°E; light gray), zonal wind (U850) over northern Indian subcontinent (NI; 20°–30°N, 70°–90°E; blue), and sea surface temperature (SST) in Niño.3.4 region (N34; 5°S–5°N, 170°–120°W; deep gray). Note that NI and N34 indices were multiplied by “–1”. The black solid and dashed lines (refer to right y axis) are normalized indices of precipitation (PR; from GPCP) and land-only precipitation (PR-land; from CRU) averaged over Pakistan (PKT; 22°–32°N, 63°–73°E), respectively.

southerly flow from the Arabian Sea (which was further amplified by an upward trend), resulting in a strong convergence of moisture flux, promoting the development of intense convection and heavy rainfall. The third and prolonged surge in August was particularly influenced by the interaction between an unusually warm-moist southerly flow from the Arabian Sea and an extratropical cold-dry northerly anomaly associated with upstream Europe blocking. Furthermore, the tropical–extratropical interaction played a significant role, contributing approximately 50% of the total rainfall during the third surge.

It is important to note that these contributing factors generally occur independently and rarely coincide simultaneously, which explains the infrequency of such extreme events. We argue that only when these compounding factors occur concurrently can they lead to the manifestation of extreme events²⁶. As demonstrated in Fig. 7, the proposed factors, including the anomalous mid-upper geopotential heights in Europe and central China, the 850-hPa meridional moisture flux over the Arabian Sea, the easterly winds over the northern Indian subcontinent, and the sea surface temperature in the Niño.3.4 region, synchronized and reached unusually high values in 2022, setting it apart from other years. This was also the case in the 2010 Pakistan flooding event, as well as in the extremely dry 1987 when all factors synchronized in a negative phase.

Notably, the SSTA in the Niño.3/Niño.3.4 regions exhibited fluctuations throughout the period of 2020–2022, with the July–August averaged SSTA in these regions being relatively weaker and more confined to the east in 2021 compared to 2022 and 2020 (not shown). This likely limited the impact of the 2021 La Niña on the rainfall in Pakistan, in contrast to the impacts observed in 2022 and 2020. Furthermore, a noteworthy difference in the SSTA of 2022, as compared to those in 2020 and 2021, was the westward shift of negative and stronger SSTA. This westward shift was more influential in 2022 than in the other 2 years.

The concurrence of flooding in Pakistan and the heatwave in central China suggests a potential mutual enhancement between wet and dry extremes. Our analysis supports this hypothesis by revealing a potential positive feedback between the two extremes (Fig. 4 and Supplementary Fig. 5). Specifically, the ascending motion associated with flooding in Pakistan and the descending motion associated with the heatwave in China were coupled.

Numerical experiments indicate that the anomalous rainfall in Pakistan may trigger an upper-level anticyclone downstream, strengthening the anticyclone associated with the China heatwave. Conversely, the upper-level anticyclonic anomaly associated

with the heatwave exhibited an equivalent barotropic structure, with an associated easterly anomaly extending from the upper troposphere to the lower troposphere (not shown). This easterly anomaly was suggested to be correlated with the ascending motion in Pakistan¹. However, the specific feedback processes between the China heatwave and Pakistan rainfall remain unclear and require further investigation.

The equivalent barotropic vertical structure is typical for extratropical Rossby wave-like perturbations, suggesting the extratropical origin of the anomalous anticyclone as part of the teleconnection pattern shown in Fig. 4d. The compounding effect of extratropical and La Niña-associated perturbations, with the upper-level components over central China potentially further enhanced by diabatic heating over Pakistan, contributes to the complexity of the interaction. However, the exact nature of how the China heatwave influences the Pakistan rainfall remains uncertain and warrants additional research.

The regression analysis and wave activity flux revealed a teleconnection between the Europe blocking, flooding in Pakistan, and the heatwave in China, which is mediated by a stationary Rossby wave-like pattern. This wave-like structure is distinct from the SCA and CGT patterns. We noted some similarities between this wave-like structure and the BOC pattern⁴. However, some substantial differences were identified. It remains uncertain whether these patterns are precisely the same. Further investigation is required. The occurrence of climate extremes in Europe, Pakistan, and China, similar to the 2022 event, may become more frequent if this wave-like pattern becomes more active in the future, particularly under warmer conditions. Further investigation is needed to understand the mechanism driving this wave-like pattern and its potential impacts on climate extremes across the Eurasian continent.

It has been reported that weather and climate extreme events are expected to increase in frequency and intensity as a result of a warming climate^{35,36}. Our findings suggest that the record rainfall observed in Pakistan in 2022 may be a footprint of a warming climate. The enhanced southwesterly flow over the Arabian Sea, which played a critical role in facilitating strong moisture flux convergence, and this enhancement can be attributed to recent trends. Under an extreme warming climate, further investigation is needed to understand the potential changes in the southwesterly flow over the Arabian Sea and its possible impact on tropical–extratropical interaction and extreme weather events in these regions.

METHODS

Data

We used the daily precipitation data (with horizontal resolution of $0.5^\circ \times 0.5^\circ$) from the Climate Prediction Center (CPC) Global Unified-Based Analysis of Daily Precipitation³⁷ and monthly precipitation data (with horizontal resolution of $2.5^\circ \times 2.5^\circ$) from the Global Precipitation Climatology Project³⁸ (GPCP; version 2.3) and Climatic Research Unit gridded Time Series³⁹ (CRU; version ts4.07). We utilized the ERA5 daily and monthly data⁴⁰, including horizontal winds, geopotential height, and specific humidity, of the European Centre for Medium-Range Weather Forecasts in diagnostics. The original horizontal resolution of ERA5 data is $0.25^\circ \times 0.25^\circ$. For consistency of calculation and coordination of figures, we regridded the ERA5 data to a horizontal resolution of $2.5^\circ \times 2.5^\circ$. In addition, we used monthly sea surface temperature data (with horizontal resolution of $2^\circ \times 2^\circ$) of the Extended Reconstructed Sea Surface Temperature⁴¹ (ERSST, version 5) and daily interpolated outgoing longwave (OLR) radiation data (with horizontal resolution of $2.5^\circ \times 2.5^\circ$) of NOAA⁴².

Blocking index

Blocking index⁴³ was calculated to identify atmospheric blocking that often accompanies prolonged heatwaves. For the Northern Hemisphere, the blocking index (BI) was defined based on the 500-hPa geopotential height gradient south:

$$BI = (Z(\lambda, \varphi_o) - Z(\lambda, \varphi_s)) / (\varphi_o - \varphi_s), \quad (1)$$

$$\varphi_o = 60^\circ N + \Delta, \quad (2)$$

$$\varphi_s = 40^\circ N + \Delta, \quad (3)$$

$$\Delta = -5^\circ, -2.5^\circ, 0^\circ, 2.5^\circ, 5^\circ \quad (4)$$

where Z is 500-hPa geopotential height, λ and φ is longitude and latitude, respectively. A blocking is identified at a given longitude and a specific time when at least one value of Δ satisfy that $BI > 0$ (units: m/degree latitude).

Heatwave index

We first calculated the value of 95th percentile of daily averaged 2-m temperature at each grid during 1979–2022. The heatwave index was then defined as the total number of grids exceeding the 95th percentile in the $20^\circ N$ – $40^\circ N$, $80^\circ E$ – $120^\circ E$ region.

Statistical test of correlation coefficient

The Fisher's Z-transformation was used for the statistical test of the Pearson correlation coefficient.

Regression analysis

We calculated regression coefficients to estimate the relationship between two monthly mean time series. The linear regression model is expressed as $Y_i = \alpha + \beta X_i + \varepsilon$, where X_i and Y_i are variables being examined, α is the intercept, β is the slope (regression coefficient), and ε is the residual.

Percentile rank

The percentile rank is expressed as a whole number between 1 and 99 and is used to evaluate the precipitation intensity and T2m as the percentage of scores in a reference group that is lower than a given score of interest.

Idealized heating experiments

We used the LBM to conduct idealized heating experiments⁴⁴. The model was forced by an idealized heating over Pakistan

(centering at $29^\circ N$, $68^\circ E$) to simulate atmospheric responses in the August climatological background flow. The 200- and 850-hPa geopotential heights and horizontal winds from the day-30 output were analyzed.

DATA AVAILABILITY

The CPC and GPCP precipitation data were provided by NOAA/OAR/ESRL PSL, Boulder, Colorado, USA, from their websites at <https://psl.noaa.gov/data/gridded/data.cpc.globalprecip.html> and <https://psl.noaa.gov/data/gridded/data.gpcp.html>, respectively. The ERA5 reanalysis data was obtained from Copernicus Climate Change Service (C3S) Climate Data Store (CDS) and is available at <https://cds.climate.copernicus.eu/cdsapp#!/dataset/reanalysis-era5-pressure-levels-monthly-means?tab=form>. The ERSST sea surface data was from <https://psl.noaa.gov/data/gridded/data.noaa.ersst.v5.html>. The NOAA interpolated outgoing longwave radiation data was from <https://psl.noaa.gov/data/gridded/data.olrldr.interp.html>.

CODE AVAILABILITY

All the computer codes used to generate the results and figures in this study are available from the authors upon request. All figures were generated by using the MATLAB and Statistics Toolbox Release 2021b version 9.11.0.1769968 with the M_MAP mapping package version 1.4 m (<https://www.eoas.ubc.ca/~rich/map.html>), and the NCAR Command Language (NCL) (<https://www.ncl.ucar.edu/>) version 6.3.0.

Received: 22 May 2023; Accepted: 27 September 2023;

Published online: 14 October 2023

REFERENCES

- He, C., Zhou, T., Zhang, L., Chen, X. & Zhang, W. Extremely hot East Asia and flooding western South Asia in the summer of 2022 tied to reversed flow over Tibetan Plateau. *Clim. Dyn.* **61**, 2103–2119 (2023).
- Saji, N. H. & Yamagata, T. Structure of SST and surface wind variability during Indian Ocean dipole mode events: COADS observations. *J. Clim.* **16**, 2735–2751 (2003).
- Ashok, K., Chan, W.-L., Motoi, T. & Yamagata, T. Decadal variability of the Indian Ocean dipole. *Geophys. Res. Lett.* **31**, L24207 (2004).
- Kripalani, R. H. & Kumar, P. Northeast monsoon rainfall variability over south peninsular India vis-à-vis the Indian Ocean dipole mode. *Int. J. Climatol.* **24**, 1267–1282 (2004).
- Kripalani, R. H., Oh, J.-H., Kang, J.-H., Sabade, S. S. & Kulkarni, A. Extreme monsoons over East Asia: possible role of Indian Ocean zonal mode. *Theor. Appl. Climatol.* **82**, 81–94 (2005).
- Hong, C.-C., Lu, M.-M. & Kanamitsu, M. Temporal and spatial characteristics of positive and negative Indian Ocean dipole with and without ENSO. *J. Geophys. Res.* **113**, D08107 (2008).
- Hong, C.-C., Hsu, H.-H., Lin, N.-H. & Chiu, H. Roles of European blocking and tropical-extratropical interaction in the 2010 Pakistan flooding. *Geophys. Res. Lett.* **38**, L13806 (2011).
- Khalid, B. et al. Riverine flood assessment in Jhang district in connection with ENSO and summer monsoon rainfall over Upper Indus Basin for 2010. *Nat. Hazards* **92**, 971–993 (2018).
- Lau, W. K. M. & Kim, K.-M. The 2010 Pakistan flood and Russian heat wave: teleconnection of hydrometeorological extremes. *J. Hydrometeorol.* **13**, 392–403 (2012).
- Martius, O. et al. The role of upper-level dynamics and surface processes for the Pakistan flood of July 2010. *Q. J. R. Meteorol. Soc.* **139**, 1780–1797 (2013).
- Zheng, J. & Wang, C. Hot Summers in the Northern Hemisphere. *Geophys. Res. Lett.* **46**, 10891–10900 (2019).
- Hong, C.-C., Tseng, W.-L., Hsu, H.-H., Lee, M.-Y. & Chang, C.-C. Relative contribution of trend and interannually varying SST anomalies to the 2018 heat waves in the extratropical northern hemisphere. *J. Clim.* **34**, 6319–6333 (2021).
- Perkins, S. E., Alexander, L. V. & Nairn, J. R. Increasing frequency, intensity and duration of observed global heatwaves and warm spells. *Geophys. Res. Lett.* **39**, L20714 (2012).
- Zampieri, M. et al. Global assessment of heat wave magnitudes from 1901 to 2010 and implications for the river discharge of the Alps. *Sci. Total Environ.* **571**, 1330–1339 (2016).
- Luo, J.-J., Sasaki, W. & Masumoto, Y. Indian Ocean warming modulates Pacific climate change. *Proc. Natl Acad. Sci. USA* **109**, 18701–18706 (2012).
- Abish, B., Cherchi, A. & Ratna, S. B. ENSO and the recent warming of the Indian Ocean. *Int. J. Climatol.* **38**, 203–214 (2018).

17. Yuan, Y. et al. The 2016 summer floods in China and associated physical mechanisms: a comparison with 1998. *J. Meteorol. Res.* **31**, 261–277 (2017).
18. Lee, M.-Y., Hong, C.-C. & Hsu, H.-H. Compounding effects of warm sea surface temperature and reduced sea ice on the extreme circulation over the extratropical North Pacific and North America during the 2013–2014 boreal winter. *Geophys. Res. Lett.* **42**, 1612–1618 (2015).
19. Nanditha, J. S. et al. The Pakistan flood of August 2022: causes and implications. *Earth's Future* **11**, e2022EF003230 (2023).
20. Enomoto, T., Hoskins, B. J. & Matsuda, Y. The formation mechanism of the Bonin high in August. *Q. J. R. Meteorol. Soc.* **129**, 157–178 (2003).
21. Chang, C.-P., Zhang, Y. & Li, T. Interannual and interdecadal variations of the East Asian summer monsoon and tropical Pacific SSTs. Part I: roles of the subtropical ridge. *J. Clim.* **13**, 4310–4325 (2000).
22. Jiang, X., Li, Y., Yang, S. & Wu, R. Interannual and interdecadal variations of the South Asian and western Pacific subtropical highs and their relationships with Asian-Pacific summer climate. *Meteorol. Atmos. Phys.* **113**, 171–180 (2011).
23. Webster, P. J. & Yang, S. Monsoon and ENSO: selectively interactive systems. *Q. J. R. Meteorol. Soc.* **118**, 877–926 (1992).
24. Kripalani, R. H. & Kulkarni, A. Climatic impact of El Niño/La Niña on the Indian monsoon: a new perspective. *Weather* **52**, 39–46 (1997).
25. Yadav, R. K. Role of equatorial central Pacific and northwest of North Atlantic 2-metre surface temperatures in modulating Indian summer monsoon variability. *Clim. Dyn.* **32**, 549–563 (2009).
26. Zscheischler, J. et al. A typology of compound weather and climate events. *Nat. Rev. Earth Environ.* **1**, 333–347 (2020).
27. Hong, C.-C., Lee, M.-Y., Hsu, H.-H., Lin, N.-H. & Tsuang, B.-J. Tropical SST forcing on the anomalous WNP subtropical high during July–August 2010 and the record-high SST in the tropical Atlantic. *Clim. Dyn.* **45**, 633–650 (2015).
28. Trenberth, K. E. & Fasullo, J. T. Climate extremes and climate change: the Russian heat wave and other climate extremes of 2010. *J. Geophys. Res.: Atmos.* **117**, D17103 (2012).
29. Barnston, A. G. & Livezey, R. E. Classification, seasonality and persistence of low-frequency atmospheric circulation patterns. *Mon. Weather Rev.* **115**, 1083–1126 (1987).
30. Bueh, C. & Nakamura, H. Scandinavian pattern and its climatic impact. *Q. J. R. Meteorol. Soc.* **133**, 2117–2131 (2007).
31. Li, M., Yao, Y., Luo, D. & Zhong, L. The linkage of the large-scale circulation pattern to a long-lived heatwave over Mideastern China in 2018. *Atmosphere* **10**, 89 (2019).
32. Ding, Q. & Wang, B. Circumglobal teleconnection in the northern hemisphere summer. *J. Clim.* **18**, 3483–3505 (2005).
33. Xu, P. et al. The British–Okhotsk corridor pattern and its linkage to the Silk Road pattern. *J. Clim.* **35**, 5787–5804 (2022).
34. Takaya, K. & Nakamura, H. A formulation of a phase-independent wave-activity flux for stationary and migratory quasigeostrophic eddies on a zonally varying basic flow. *J. Atmos. Sci.* **58**, 608–627 (2001).
35. Berg, P., Moseley, C. & Haerter, J. O. Strong increase in convective precipitation in response to higher temperatures. *Nat. Geosci.* **6**, 181–185 (2013).
36. Myhre, G. et al. Frequency of extreme precipitation increases extensively with event rareness under global warming. *Sci. Rep.* **9**, 16063 (2019).
37. Chen, M. et al. Assessing objective techniques for gauge-based analyses of global daily precipitation. *J. Geophys. Res.: Atmos.* **113**, D04110 (2008).
38. Adler, R. et al. The global precipitation climatology project (GPCP) monthly analysis (new version 2.3) and a review of 2017 global precipitation. *Atmosphere* **9**, 138 (2018).
39. Harris, I., Osborn, T. J., Jones, P. & Lister, D. Version 4 of the CRU TS monthly high-resolution gridded multivariate climate dataset. *Sci. Data* **7**, 109 (2020).
40. Hersbach, H. et al. The ERA5 global reanalysis. *Q. J. R. Meteorol. Soc.* **146**, 1999–2049 (2020).
41. Huang, B. et al. Extended reconstructed sea surface temperature, version 5 (ERSSTv5): upgrades, validations, and intercomparisons. *J. Clim.* **30**, 8179–8205 (2017).
42. Liebmann, B. & Smith, C. A. Description of a complete (interpolated) outgoing longwave radiation dataset. *Bull. Am. Meteorol. Soc.* **77**, 1275–1277 (1996).
43. Tibaldi, S. & Molteni, F. On the operational predictability of blocking. *Tellus A Dyn. Meteorol. Oceanogr.* **42**, 343–365 (1990).
44. Watanabe, M. & Kimoto, M. Atmosphere–ocean thermal coupling in the North Atlantic: a positive feedback. *Q. J. R. Meteorol. Soc.* **126**, 3343–3369 (2000).

ACKNOWLEDGEMENTS

This study was in memory of Dr. Masao Kanamitsu, who gave C.-C.H. a crucial push in his first research visit. This study was supported by the National Science and Technology Council (NSTC), Taiwan (R.O.C.), under grant numbers 109-2111-M-845-001, 110-2111-M-845-001, 111-2625-M-845-001, and 111-2811-M-001-093. The authors are grateful to the National Center for High-Performance Computing (NCHC), National Applied Research Laboratories (NARLabs) for providing computer facilities. This manuscript was edited by Wallace Academic Editing.

AUTHOR CONTRIBUTIONS

C.-C.H. and H.-H.H. conceptualized the study. A.-Y.H. and C.-C.C. contributed to data analysis. W.-L.T. conducted model experiments. C.-C.H. prepared the first draft, H.-H.H. provided critical suggestions in revision, and A.-Y.H. and M.-M.L. participated in revision. All authors contributed to review and improve the manuscript and approve the final manuscript.

COMPETING INTERESTS

The authors declare no competing interests.

ADDITIONAL INFORMATION

Supplementary information The online version contains supplementary material available at <https://doi.org/10.1038/s41612-023-00492-2>.

Correspondence and requests for materials should be addressed to Huang-Hsiung Hsu.

Reprints and permission information is available at <http://www.nature.com/reprints>

Publisher's note Springer Nature remains neutral with regard to jurisdictional claims in published maps and institutional affiliations.



Open Access This article is licensed under a Creative Commons Attribution 4.0 International License, which permits use, sharing, adaptation, distribution and reproduction in any medium or format, as long as you give appropriate credit to the original author(s) and the source, provide a link to the Creative Commons license, and indicate if changes were made. The images or other third party material in this article are included in the article's Creative Commons license, unless indicated otherwise in a credit line to the material. If material is not included in the article's Creative Commons license and your intended use is not permitted by statutory regulation or exceeds the permitted use, you will need to obtain permission directly from the copyright holder. To view a copy of this license, visit <http://creativecommons.org/licenses/by/4.0/>.

© The Author(s) 2023